Article

Permeability Study of Austenitic Stainless Steel Surfaces Produced by Selective Laser Melting

Emmanuel Segura-Cardenas [1], Erick Ramirez-Cedillo [1], Jesús Alejandro Sandoval-Robles [1], Leopoldo Ruiz-Huerta [2], Alberto Caballero-Ruiz [2] and Hector R. Siller [3,*]

[1] Tecnologico de Monterrey, Escuela de Ingeniería y Ciencias, Avenida Eugenio Garza Sada #2501 Sur, Monterrey, Nuevo Leon 64849, Mexico; esca@itesm.mx (E.S.-C.); a00806274@itesm.mx (E.R.-C.); jesus.sandoval@itesm.mx (J.A.S.-R.)

[2] Laboratorio Nacional de Manufactura Aditiva, Digitalización 3D y Tomografía Computarizada, MADiT, Centro de Ciencias Aplicadas y Desarrollo Tecnológico (CCADET), Universidad Nacional Autónoma de México (UNAM), Circuito Exterior S/N, Ciudad Universitaria AP 70-186, Ciudad de México 04510, Mexico; leoruiz@unam.mx (L.R.-H.); alberto.caballero@ccadet.unam.mx (A.C.-R.)

[3] Department of Engineering Technology, University of North Texas, 3940 North Elm Street, Denton, TX 76207, USA

[*] Correspondence: hector.siller@unt.edu; Tel.: +1-940-565-2362

Abstract: Selective laser melting (SLM) is emerging as a versatile process for fabricating different metal components with acceptable mechanical properties and geometrical accuracy. The process has been used in the manufacturing of several parts (e.g., aerospace or biomedical components), and offers the capability to tailor the performance of several surface and mechanical properties. In this work, permeability properties and surface roughness of stainless steel (SS316L) surfaces were evaluated through experimentation with three different laser scanning patterns (chessboard, meander, and stripe), and different sloping angles between the fabricated surface and the laser beam incident on the process. Results showed that for each scanning pattern, the roughness decreased as the sloping angle increased consistently in all experimental trials. Furthermore, in the case of the permeability evaluation, the manufactured surfaces showed changes in properties for each series of experiments performed with different scanning patterns. The chessboard pattern showed a change of 67° to 107° in contact angle, while the meander and stripe patterns showed a variation in contact angle in a range of 65° to 85°. The different scanning strategies in the SLM process resulted in an alternative method for surface enhancement with different hydrophobicity properties, valuable for designing the most appropriate permeability characteristics for specific applications.

Keywords: selective laser melting; stainless steel; surface quality; permeability

1. Introduction

Selective laser melting (SLM) technology is an additive manufacturing (AM) process that enables the fabrication of components with complex shapes for medical, aerospace, and automotive applications directly from metal powder [1–3], offering a series of advantages compared with traditional processing techniques due to its versatility in producing both metal and polymer parts [4–7]. The SLM process enables the direct melting of powders of a number of alloys, such as titanium (Ti6Al4V), stainless steel (SS316L), cobalt-chromium (Co-Cr), aluminum, and the building of net-shape parts through a layer-by-layer process. For each layer, a scanning laser beam supplies the energy to melt a layer of deposited metal powder and fuse it onto a previously melted layer.

The use of SLM technologies is now an asset in the manufacturing of biomedical devices [8,9], due to its use for customizing medical implants and orthodontic devices to the patient's anatomy. Another [10,11] increasing application is the development of aeronautic components with high degrees of shape complexity. However, SLM still faces limitations in terms of surface quality when it is compared to some conventional metal manufacturing processes. Surface quality is significantly influenced by the stair step effect resulting from the building angle measured from the building plate to the building orientation, which is the stepped approximation by layers of curved and inclined surfaces [12]. This effect is present to a greater or lesser degree in all additive layer-manufacturing processes as consequence of the manufacturing process and the layer discretization. Surface quality (surface roughness, corrosion, and porosity properties) is also influenced by process parameters such as temperature profiles and densification ratios, among others [13–16]. However, the layer thickness can be reduced in order to improve the surface finish [17], but a smooth surface is also constrained by the balling phenomenon, which refers to the particles either not melting at all or joining into rather large droplets, which occurs during laser melting [18–20]. The balling phenomenon is related to the wettability of the powder; a poor wettability of the working powder increases the probability of developing this undesirable effect. The wettability also affects the mechanical and corrosion behavior of the fabricated parts, so it is considered as an important element to be consider in selective laser melting effectiveness. Poor wettability in the surface produces cracks that will further cause catastrophic failures in mechanical functional components [21]. Thus, it can be determined that laser-melted surfaces with good wettability are less prone to corrosion and have higher wear resistance in comparison with damaged surfaces.

The balling effect limits the laser melting process resolution because it causes the formation of discontinuous tracks, therefore limiting the formation of accurate geometries. The ability to control the wetting properties of metal alloys is extremely beneficial, in many areas for scientific and industrial applications. Wetting controllability includes the enhancement of heat transfer [22–24], improvement of surface coatings [25], and self-cleaning and anti-icing surface fabrications [26,27]. An alternative way to control wettability is the use of conical microstructures formed by the irradiation of surfaces with femtosecond laser pulses, in order to modify their properties for conducting contact angle evaluations [28,29].

Other methods have been employed to control the wetting properties of surfaces for preparing (a) hydrophilic surfaces via hydrophilic coatings [21,22], plasma treatments [23,24], or chemical treatments [25] and (b) hydrophobic surfaces via hydrophobic coatings [27,30–33]. However, these methods are generally expensive, complicated, and time consuming. Some simple methods, such as chemical treatments and inexpensive coatings are generally either evanescent or fragile. Moreover, no single method can cover the wide range of contact angles from the super-hydrophilic to super-hydrophobic condition.

SLM is capable of processing a variety of materials, and the development of powders is growing in variety. Accordingly, the research with metal alloys suitable for broad applications may be a better example for industrial scenarios. Stainless steel alloys accomplish this requirement since they may be used for biomedical device manufacturing, automotive component fabrication, and oil and gas instrumentation, among other applications [34,35]. Furthermore, there are few studies related to the permeability of stainless steels. Chemical processes have been useful in controlling the hydrophobic characteristics of these alloys [36]. On the other hand, Antony et al. [37] focus their studies of permeability by modifying scanning speeds and laser power during the melting process. Accordingly, it is well known after reviewing the literature that process parameters can be modified in order to change the final part properties, and thus eliminating conventional post-processing steps for the preparation of surfaces with good wettability. In order to contribute towards the complete evaluation of SLM in the manufacturing of functional surfaces, this study is intended to propose an alternative methodology for modifying the wettability of surfaces obtained by the process using different laser scanning strategies.

2. Materials and Methods

In order to perform a set of experiments for surface properties modification, a powder bed selective laser melting system was used. This system (Renishaw, Gloucestershire, UK) allows the manufacture of metal parts within a volume of 250 mm × 250 mm × 300 mm. The radiation source was a laser Yb-fiber with a maximum power of P = 400 W, a wavelength of λ = 1075 nm, and a spot size of d = 113 μm. The thickness of the layer was 50 μm, and the powder used was austenitic stainless steel (designation SS 316L-0410, Renishaw, Gloucestershire, UK) with the following composition: Fe (Bal), Cr (16–18%), Ni (10–14%), Mo (2–3%), Mn (<2%), Si (<0.1%), N (<0.1%), O (<0.1%), P (0.045%), C (0.03%), S (0.03%).

The distribution of particles size was calculated with the aid of scanning electron microscope (SEM) micrographs and with the use of image analysis software (imageJ, National Institutes of Health, 1.51r, Bethesda, MD, USA). After laser beam scanning of each cross-section, the manufacturing plate was lowered by the thickness of the layer to be deposited, thus maintaining the surface in the focal plane. Parts of 10 mm × 10 mm × 5 mm were fabricated at different sloping angles (θ) with respect to the normal laser beam (θ = 0°, 45°, 60°, 70°, 90°) as it is represented in Figure 1. Additionally, Table 1 shows the parameters used in the SLM process. After the manufacturing process, the samples were removed from the building plate and were brought to a cleaning process in an ultrasonic bath for 10 min in 95% ethanol, 10 min in acetone, and dried. The morphology and particle size distribution (30 images obtained) of the samples were carefully analyzed by using an EVO MA25 ZEISS scanning electron microscope (ZEISS, German, Jena, Germany). The surface roughness and contact angle measurements were made after each experimental run, as it is explained in the following.
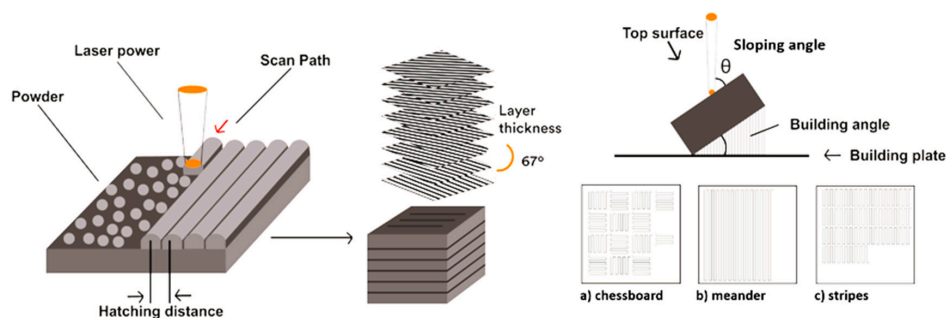

Figure 1. Laser scanning of stainless steel 316L using selective laser melting (SLM) (right). Orientation of the samples and sloping angle (top left) and scanning laser types: (**a**) chessboard, (**b**) meander, (**c**) stripes (down left).

Table 1. Process parameters for Stainless steel 316L.

Parameter	Value
Laser Power (W)	200
Layer Thickness (μm)	50
Scan speed (mm/s)	2000
Hatch spacing (mm)	0.115
Energy density (J/mm^2)	0.884

2.1. Contact Angle (CA)

Contact angle (CA) measured from the surface of a building part and a droplet of water was performed to evaluate the permeability characteristics of the fabricated parts [38]. The contact angle has been drawn by the Dataphysics OCA 15EC system (DataPhysics Instruments GmbH, Filderstadt, Germany) in the measurement range of 1–180°. The evaluation of the drop shape and the calculation of the contact angle (Figure 2B) were performed with the aid of the SCA20_U software (DataPhysics

Instruments GmbH, SCA 20, Filderstadt, Germany). 10 μL of drops were placed onto the substrate using an automatic dispenser, and were injected slowly at 2 μL/s onto the solid surface by a syringe (Figure 2A). To measure contact angle values, droplet images were taken directly after 8 s of deposition in order to eliminate the impact of droplet evaporation (Figure 2B). The value of CA is the average of CA right and CA left. The contact angle tests were carried out at 23 °C.
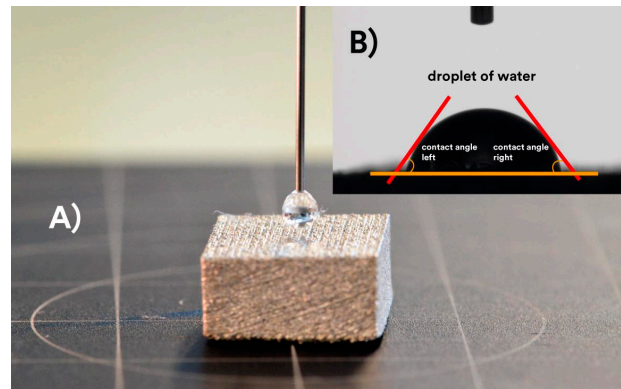

Figure 2. Contact angle configuration: (**A**) Stainless 316L surface and water drop; (**B**) Contact angle analysis.

2.2. Roughness

In order to characterize surface roughness (Ra), samples were oriented in different angles with respect to the building plate, and different building patterns were used. The average surface roughness (Ra) measurements were performed using the ISO 4287 standard, which is one of the most adopted texture parameters in the literature [39,40]. For this study, a non-contact 3D profilometry method was used. The surface topography information of the top surfaces of the samples was obtained using a focus variation Alicona infinite focus microscope G4 (Alicona Imaging GmbH, Graz, Austria). It was used with an objective with 20× magnification, with a vertical resolution of 50 μm and lateral resolution of 3.5 μm. Ra values were calculated with a cut-off length of 2500 μm. This cut-off captured the overall surface roughness, allowing the high-frequency roughness oscillations to be detected from the low-frequency waveforms [19]. Three sections were selected in the samples (top, center, and bottom), so that subsequently three measurements were made (top, center, and bottom).

3. Results and Discussion

3.1. Scanning Electron Microscope

The particle size distribution obtained from the SEM images is shown in Figure 3, where it can be seen that the majority of the particles presented a spherical shape. The size distribution was found to be between 7 and 55 μm, with an average diameter of ~25 μm and D50 = 27.79 μm.

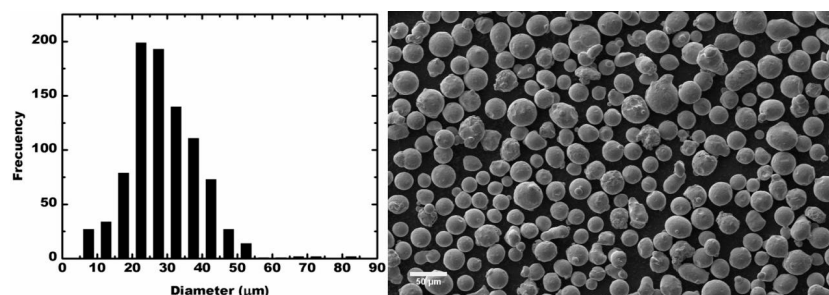**Figure 3.** Particles distribution.

For the surface morphology characterization, SEM analysis was carried out at θ = 90° and 60°, and for the three laser scanning strategies. Figure 4a–c shows a few partially sintered particles attached on the surface, where it can be seen that smoothed uniform layers were obtained in the process under these conditions. As θ increases, the sharpness of the edges diminishes due to the increase of unsintered particles that are trapped, and remain between the layers (Figure 4d–f). The formation of discontinuous edges is partly determined by the friction effect, which occurs during laser melting of the metal powder [41]. During laser melting, heat at the edges of the layers is not enough to melt the particles; consequently, they do not fuse with the processed layer, tending to be adhered to the surface at this region as shown. Balling is a severe impediment in the layers' bonding, decreasing the density of the part and increasing the surface roughness [42]. Increasing the temperature of the powder bed can increase permeability, thereby reducing the balling phenomenon [43]. However, the scope of this work is to find the influence of the laser scanning strategies on the surface properties; thus, it is intended to contribute to the enhancement of the process in addition to other aspects in parameters modification that have been studied before.
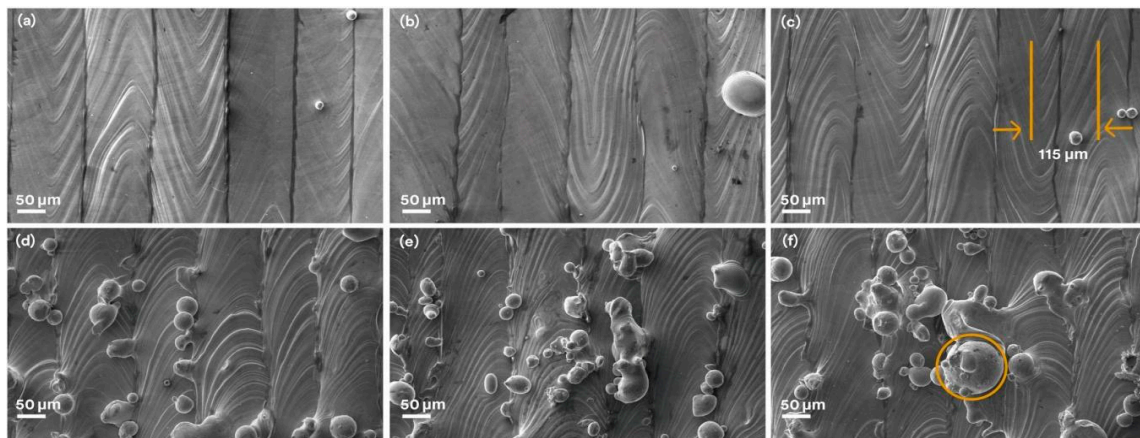

Figure 4. Scanning electron microscope (SEM) micrographs of the samples at 90°: (**a**) chessboard, (**b**) meander, and (**c**) stripes/hatching distance of 115 μm; and at 60°: (**d**) chessboard, (**e**) meander, and (**f**) stripes; the circle shows semi-molten particles which create roughness on the sintered surface.

3.2. Roughness

Roughness (Ra) was measured on the samples without post-processing with the non-contact 3D instrument described above. Figure 5 shows the average roughness values of the different laser scanning strategies employed. It can be seen that as θ increases, the surface roughness values decrease; this tendency was observed in all samples during the experimental trials. It is observed that the three scanning patterns show a similar behavior. The lowest roughness value Ra is present at θ = 90°; in this case, the laser beam is perpendicular to the scanning surface and the metal particles are almost completely melted, forming a smooth surface and decreasing the balling effect, consistent with SEM results. Chessboard laser scanning presents a greater roughness for the different θ angles used. These Ra values vary from 12 to 19 μm. Meander and stripes laser scanning have smoother surfaces, the roughness changes from 12 to 6 μm with the variation of the building angle. Some authors [13,44] have reported that roughness values Ra vary depending on the parameters used during the melting process. For this work, the authors show that chessboard laser scanning creates rougher surfaces, the scanning shape changes continuously in orientation, and the areas to be consolidated are smaller than when using a one-dimensional scan. These changes of orientation in the patterns influence the construction time and properties of SLM components and supports.
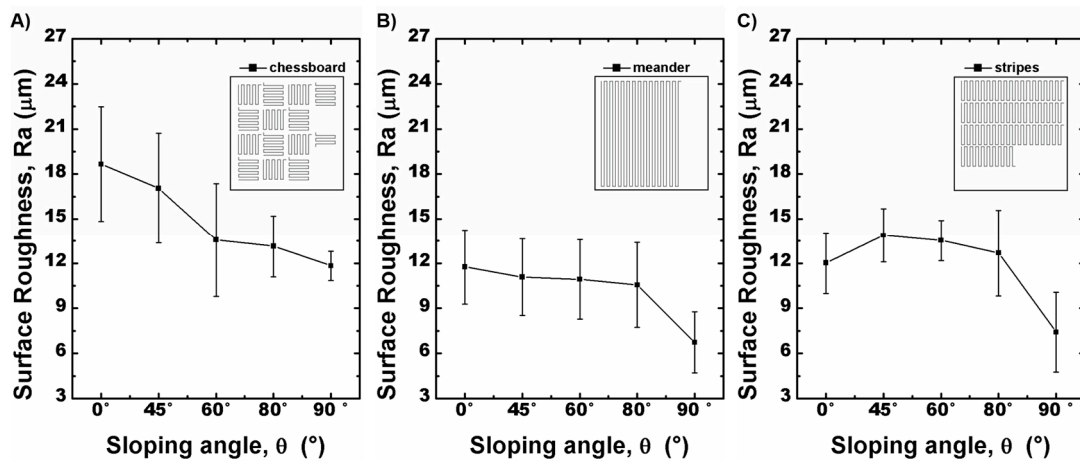
Figure 5. Surface roughness results with different scanning strategies and sloping angles: (**A**) chessboard, (**B**) meander and (**C**) stripes.

The top surfaces of the samples with the meander scanning laser path at different sloping angles $\theta = 90°$ (Figure 6A), 70° (Figure 6B), 60° (Figure 6C), 45° (Figure 6D), and 0° (Figure 6E) are presented as topographies. The measured area was defined by 1.620 mm × 1.620 mm, and height was dependent on the surface profile having values from 133.507 to 180.583 µm.
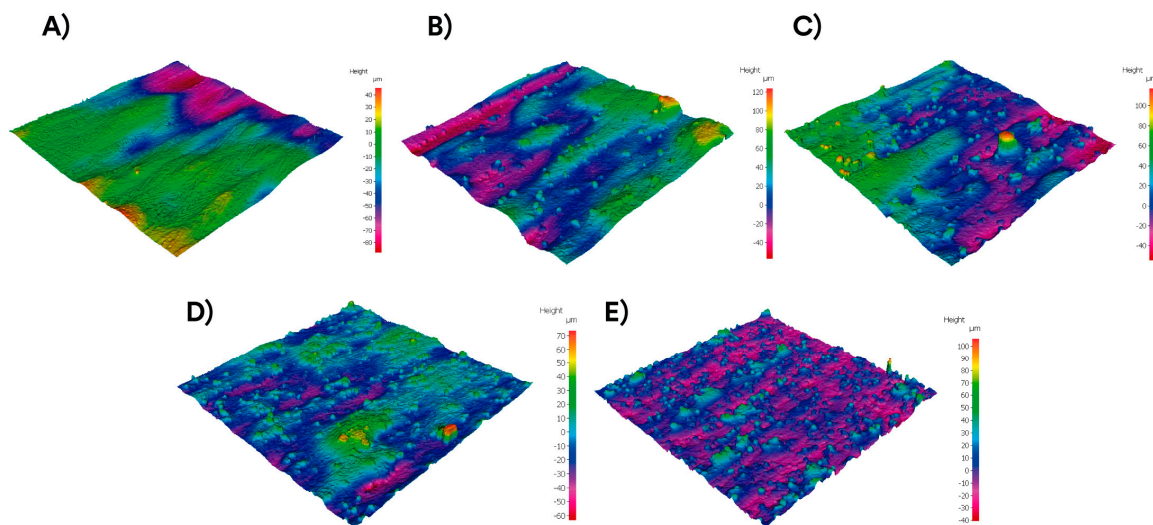

Figure 6. Top surface topographies at different sloping angle (θ) with meander scanning path. (**A**) 90°, (**B**) 70°, (**C**) 60°, (**D**) 45°, and (**E**) 0°.

3.3. Contact Angle

CA measurements were performed on the surfaces of the samples in order to observe the change in permeability for each scanning strategy used. For each measurement, the samples were analyzed under the same conditions, and five random areas of the surface of each sample were evaluated. Figure 7 shows the variation of the CA for different sloping angles and each scanning strategy; the error bars indicate the variability for each combination. It can be noticed that the equilibrium CAs at the surfaces are approximately between 70° and 120°.

It can be seen that the CAs decrease with the increase of θ. The chessboard scanning strategy shows a larger change in CA from 67° to 107° (Figure 7A). In the cases of meander and stripes scanning strategies, the behavior is similar and the variation of the CA oscillates from approximately 65° to 85° (Figure 7B,C). Some authors have associated the permeability with the roughness, but it

has been seen that materials with the same roughness have different values of CA; this shows that the permeability cannot be controlled solely by the roughness modification [45]. Other authors found that the permeability of stainless steel surfaces can be changed by modifying SLM parameters like laser power, scanning speed, and beam diameter [39]. Nevertheless, the sloping angle variation and the laser scanning strategy modification turn out to be alternative methods to control the permeability of the parts produced by SLM. The influence of the scanning strategy has been a useful tool for controlling different surface properties in the sintering process [15]. Thus, the different conditions employed for SLM show a change in hydrophobicity that is possible to control depending on the required need.
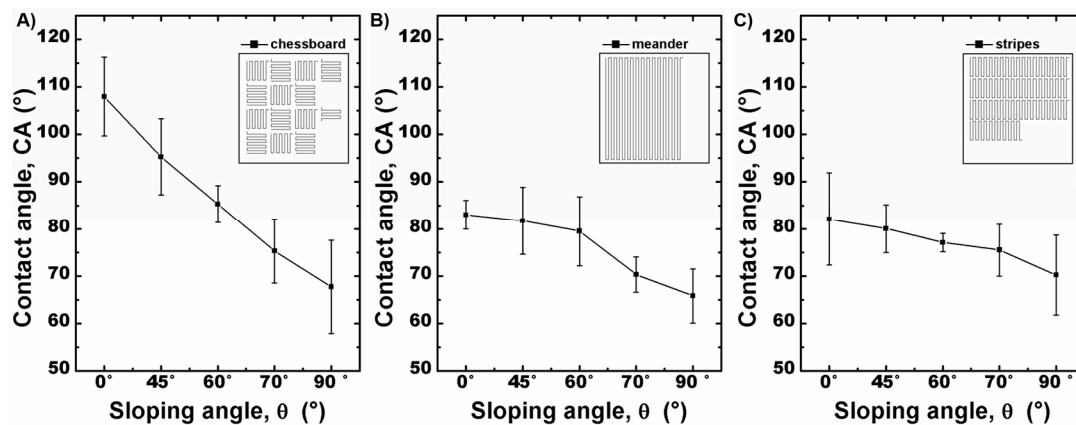

Figure 7. Contact angle measurements results with different scanning strategies and sloping angles: (**A**) chessboard, (**B**) meander and (**C**) stripes.

4. Conclusions

This work discusses the application of different laser scanning strategies in order to modify the permeability characteristics of selective laser melted surfaces made of austenitic stainless steel. The main conclusions that can be drawn are:

1. The lowest Ra values were found on the surfaces with greater sloping angle. Additionally, these surfaces present fewer desegregated particles.
2. As the sloping angle diminishes, the accumulation of semi-melted particles increases, increasing the roughness of the surface.
3. The meander and stripes scanning strategies showed one-dimensional scenes in which the balling effect is smaller with respect to the chessboard scanning laser. The chessboard scanning strategy showed a continuous change in the scanning direction in the SLM process, which generates a surface with greater roughness.
4. The layer-by-layer overlay in the SLM process showed that the one-dimensional scanning direction creates a smooth surface with a slight change in the contact angle.
5. The three conditions studied showed that the surface roughness might have the same value but different contact angles, indicating that the permeability can be controlled without a significant detriment to surface quality.

In addition to the findings in previous works, in which the surface permeability is calibrated by the variation of laser parameters in SLM, the contribution of the work presented here turns out to be an alternative methodology for the preparation of surfaces for different applications. In order to make a comprehensive assessment of selective laser melting operations for the fabrication of functional surfaces, the combination of powder materials, process parameters, surface orientation, and scanning strategies will be studied in future works, including the densification of the parts changing these parameters and its influence on the mechanical and surface development.

Author Contributions: Emmanuel Segura-Cardenas wrote the manuscript and performed the execution of part of the experimentation; Erick Guadalupe Ramirez-Cedillo performed the metrology procedures and analyzed the data; Jesús Alejandro Sandoval-Robles performed part the experimentation and developed the materials characterization; Leopoldo Ruiz-Huerta and Alberto Caballero-Ruiz contributed equally in the writing of the literature review and analyzed part of the data. Hector Rafael Siller conceived the manuscript and the objectives of the experimental work, besides of revising the final version of the manuscript.

Conflicts of Interest: The authors declare no conflict of interest. The founding sponsors had no role in the design of the study; in the collection, analyses, or interpretation of data; in the writing of the manuscript, and in the decision to publish the results.

References

1. Yadroitsev, I.; Krakhmalev, P.; Yadroitsava, I. Selective laser melting of Ti6Al4V alloy for biomedical applications: Temperature monitoring and microstructural evolution. *J. Alloys Compd.* **2014**, *583*, 404–409. [CrossRef]
2. Yap, C.Y.; Chua, C.K.; Dong, Z.L.; Liu, Z.H.; Zhang, D.Q.; Loh, L.E.; Sing, S.L. Review of selective laser melting: Materials and applications. *Am. J. Phys.* **2015**, *2*, 41101–41122. [CrossRef]
3. Mu, Y. 3D Printing of Metals. *Metals* **2016**, *7*, 403. [CrossRef]
4. Yadroitsev, I.; Bertrand, P.; Smurov, I. Parametric analysis of the selective laser melting process. *Appl. Surf. Sci.* **2007**, *253*, 8064–8069. [CrossRef]
5. Li, R.; Shi, Y.; Liu, J.; Xie, Z.; Wang, Z. Selective laser melting W-10 wt.% Cu composite powders. *Int. J. Adv. Manuf. Technol.* **2010**, *48*, 597–605. [CrossRef]
6. Jhabvala, J.; Boillat, E.; André, C.; Glardon, R. An innovative method to build support structures with a pulsed laser in the selective laser melting process. *Int. J. Adv. Manuf. Technol.* **2012**, *59*, 137–142. [CrossRef]
7. Wang, F. Mechanical property study on rapid additive layer manufacture Hastelloy X alloy by selective laser melting technology. *Int. J. Adv. Manuf. Technol.* **2012**, *58*, 545–551. [CrossRef]
8. Deing, A.; Luthringer, B.; Laipple, D.; Ebel, T.; Willumeit, R. A porous TiAl6V4 implant material for medical application. *Int. J. Biomater.* **2014**, *2014*, 904230. [CrossRef] [PubMed]
9. Taniguchi, N.; Fujibayashi, S.; Takemoto, M.; Sasaki, K.; Otsuki, B. Effect of pore size on bone in growth into porous titanium implants fabricated by additive manufacturing: An in vivo experiment. *Mater. Sci. Eng. C* **2016**, *59*, 690–701. [CrossRef] [PubMed]
10. Brandt, M.; Sun, S.J.; Leary, M.; Feih, S.; Elambasseril, J.; Liu, Q.C. High-Value SLM Aerospace Components: From Design to Manufacture. *Adv. Mater. Res.* **2013**, *633*, 135–147. [CrossRef]
11. Seabra, M.; Azevedo, J.; Araújo, A.; Reis, L.; Pinto, E.; Alves, N. Selective laser melting (SLM) and topology optimization for lighter aerospace components. *Procedia Struct. Integr.* **2016**, *1*, 289–296. [CrossRef]
12. Strano, G.; Hao, L.; Everson, R.M.; Evans, K.E. Surface roughness analysis, modelling and prediction in selective laser melting. *J. Mater. Process. Technol.* **2013**, *213*, 589–597. [CrossRef]
13. Fischer, P.; Romano, V.; Weber, H.P.; Karapatis, N.P.; Boillat, E.; Glardon, R. Sintering of commercially pure titanium powder with a Nd:YAG laser source. *Acta Mater.* **2003**, *51*, 1651–1662. [CrossRef]
14. Campbell, R.I.; Martorelli, M.; Lee, H.S. Surface roughness visualisation for rapid prototyping models. *Comput. Aided Des. Appl.* **2002**, *34*, 717–725. [CrossRef]
15. Kruth, J.P.; Badrossamay, M.; Yasa, E.; Deckers, J.; Thijs, L.; Van Humbeeck, J. Part and material properties in selective laser melting of metals. In Proceedings of the 16th International Symposium on Electromachining, Shanghai, China, 19–23 April 2010.
16. Yusuf, S.; Chen, Y.; Boardman, R.; Yang, S.; Gao, N. Investigation on Porosity and Microhardness of 316L Stainless Steel Fabricated by Selective Laser Melting. *Metals* **2017**, *7*, 64. [CrossRef]
17. Dadbakhsh, S.; Hao, L. Effect of Layer Thickness in Selective Laser Melting on Microstructure of Al/5 wt % Fe_2O_3 Powder Consolidated Parts. *Sci. World J.* **2014**, *231*, 112–121.
18. Islam, M.; Purtonen, T.; Piili, H.; Salminen, A.; Nyrhilä, O. Temperature Profile and Imaging Analysis of Laser Additive Manufacturing of Stainless Steel. *Phys. Procedia* **2013**, *41*, 835–842. [CrossRef]

19. Gu, D.; Shen, Y. Balling phenomena during direct laser sintering of multi-component Cu-based metal powder. *J. Alloys Compd.* **2007**, *432*, 163–166. [CrossRef]

20. Tabernero, I.; Lamikiz, A.; Martínez, S.; Ukar, E.; López De Lacalle, L.N. Modelling of energy attenuation due to powder flow-laser beam interaction during laser cladding process. *J. Mater. Process. Technol.* **2012**, *212*, 516–522. [CrossRef]

21. Mumtaz, K.; Hopkinson, N. Top surface and side roughness of Inconel 625 parts processed using selective laser melting. *Rapid Prototyp. J.* **2009**, *15*, 96–103. [CrossRef]

22. McDonnell, A.M.P.; Beving, D.; Wang, A.; Chen, W.; Yan, Y. Hydrophilic and Antimicrobial Zeolite Coatings for Gravity-Independent Water Separation. *Adv. Funct. Mater.* **2005**, *15*, 336–340. [CrossRef]

23. Liu, J.; Aguilar, G.; Munoz, R.; Yan, Y. Hydrophilic zeolite coatings for improved heat transfer: A quantitative analysis. *AIChE J.* **2008**, *54*, 779–790. [CrossRef]

24. Takata, Y.; Hidaka, S.; Yamashita, A.; Yamamoto, H. Evaporation of water drop on a plasma-irradiated hydrophilic surface. *Int. J. Heat Fluid Flow* **2004**, *25*, 320–328. [CrossRef]

25. Niemi, R.; Mahiout, A.; Siivinen, J.; Mahlberg, R.; Likonen, J.; Nikkola, J.; Mannila, J.; Vuorio, T.; Johansson, L.S.; Söderberg, O.; et al. Surface pretreatment of austenitic stainless steel and copper by chemical, plasma electrolytic or CO_2 cryoblasting techniques for sol-gel coating. *Surf. Coat. Technol.* **2010**, *204*, 2424–2431. [CrossRef]

26. Patankar, N.A. Mimicking the lotus effect: Influence of double roughness structures and slender pillars. *Langmuir* **2004**, *20*, 8209–8213. [CrossRef] [PubMed]

27. Cao, L.; Jones, A.K.; Sikka, V.K.; Wu, J.; Gao, D. Anti-icing superhydrophobic coatings. *Langmuir* **2009**, *25*, 12444–12448. [CrossRef] [PubMed]

28. Zorba, V.; Persano, L.; Pisignano, D.; Athanassiou, A.; Stratakis, E.; Cingolani, R.; Tzanetakis, P.; Fotakis, C. Making silicon hydrophobic: Wettability control by two-lengthscale simultaneous patterning with femtosecond laser irradiation. *Nanotechnology* **2006**, *17*, 3234. [CrossRef]

29. Baldacchini, T.; Carey, J.E.; Zhou, M.; Mazur, E. Superhydrophobic surfaces prepared by microstructuring of silicon using a femtosecond laser. *Langmuir* **2006**, *22*, 4917–4919. [CrossRef] [PubMed]

30. Jagannathan, R.; Mehta, R.V. Continuous, Atmospheric Process to Create Organic Clusters and Nanostructured, Functional Films. *Adv. Funct. Mater.* **2006**, *16*, 633–639. [CrossRef]

31. Wang, Q.; Cui, Z.; Xiao, Y.; Chen, Q. Stable highly hydrophobic and oleophilic meshes for oil-water separation. *Appl. Surf. Sci.* **2007**, *253*, 9054–9060. [CrossRef]

32. Chen, L.J.; Chen, M.; Zhou, H.D.; Chen, J.M. Preparation of super-hydrophobic surface on stainless steel. *Appl. Surf. Sci.* **2008**, *255*, 3459–3462. [CrossRef]

33. Bhattacharya, S.; Kam, D.H.; Song, L.; Mazumder, J. Characterization of Individual Microneedles Formed on Alloy Surfaces by Femtosecond Laser Ablation. *Metall. Mater. Trans. A* **2012**, *43*, 2574–2580. [CrossRef]

34. Hashemi, P.M.; Borhani, E.; Nourbakhsh, M.S. A review on nanostructured stainless steel implants for biomedical application. *Nanomed. J.* **2016**, *3*, 202–216.

35. Saha Podder, A.; Bhanja, A. Applications of Stainless Steel in Automobile Industry. *Adv. Mater. Res.* **2013**, *794*, 731–740. [CrossRef]

36. Li, L.; Breedveld, V.; Hess, D.W. Creation of Superhydrophobic Stainless Steel Surfaces by Acid Treatments and Hydrophobic Film Deposition. *ACS Appl. Mater. Interfaces* **2012**, *4*, 4549–4556. [CrossRef] [PubMed]

37. Antony, K.; Arivazhagan, N.; Senthilkumaran, K. Studies on wettability of stainless steel 316L powder in laser melting process. *J. Eng. Sci. Technol.* **2014**, *9*, 533–544.

38. Goclawski, J.; Urbaniak-Domagala, W. The method of solid-liquid contact angle measurement using the images of sessile drops with shadows on substratum. In Proceedings of the 2007 International Conference on Perspective Technologies and Methods in MEMS Design, Lviv-Polyana, Ukraine, 23–26 May 2007. [CrossRef]

39. Król, M.; Dobrzański, L.A.; Reimann, Ł.; Czaja, I. Surface quality in selective laser melting of metal powders. *Arch. Mater. Sci. Eng.* **2013**, *60*, 87–92.

40. Frantsen, J.E.; Mathiesen, T. Specifying Stainless Steel Surface for the Brewery, Dairy and Pharmaceutical Sectors. In Proceedings of the CORROSION 2009, Atlanta, GA, USA, 22–26 March 2009.

41. Li, R.; Liu, J.; Shi, Y.; Wang, L.; Jiang, W. Balling behavior of stainless steel and nickel powder during selective laser melting process. *Int. J. Adv. Manuf. Technol.* **2012**, *59*, 1025–1035. [CrossRef]

42. Gu, H.; Gong, H.; Pal, D.; Rafi, K.; Starr, T.; Stucker, B. Influences of Energy Density on Porosity and Microstructure of Selective Laser Melted 17-4PH Stainless Steel. In Proceedings of the 24th Annual International Solid Freeform Fabrication Symposium: An Additive Manufacturing Conference, Austin, TX, USA, 12–13 August 2013.

43. Gu, D.; Shen, Y. Processing conditions and microstructural features of porous 316L stainless steel components by DMLS. *Appl. Surf. Sci.* **2008**, *255*, 1880–1887. [CrossRef]

44. Fox, J.C.; Moylan, S.P.; Lane, B.M. Effect of Process Parameters on the Surface Roughness of Overhanging Structures in Laser Powder Bed Fusion Additive Manufacturing. *Procedia CIRP* **2016**, *45*, 131–134. [CrossRef]

45. Bogacz, W.; Lemanowicz, M.; Al-Rashed, M.H.; Nakonieczny, D.; Piotrowski, T.; Wójcik, J. Impact of roughness, wettability and hydrodynamic conditions on the incrustation on stainless steel surfaces. *Appl. Therm. Eng.* **2017**, *112*, 352–361. [CrossRef]